Brazilian Journal of Physics
ISSN: 0103-9733
luizno.bjp@gmail.com
Sociedade Brasileira de Física
Brasil

Espindola, D. B.; Rodriguez, M. C.; Mariotto, C. Brenner
Photino and Gluino Production in SQED and SQCD
Brazilian Journal of Physics, vol. 43, núm. 1-2, abril, 2013, pp. 105-120
Sociedade Brasileira de Física
Sâo Paulo, Brasil

Braz J Phys (2013) 43:105–120
DOI 10.1007/s13538-013-0117-2

SBF SOCIEDADE BRASILEIRA DE FÍSICA

PARTICLES AND FIELDS

Photino and Gluino Production in SQED and SQCD

D. B. Espindola · M. C. Rodriguez · C. Brenner Mariotto

Received: 6 June 2012 / Published online: 12 February 2013

Abstract This review starts out with a brief history of the photino–gluino phenomenology. Next, it describes difficulties encountered in the construction of Feynman amplitudes when dealing with Majorana fermions and outlines a procedure that circumvents this difficulty by means of a prescription based on a well-defined fermion flow without explicit charge–conjugation matrices at the vertex equations. Finally, as an illustration, it calculates the cross section for the production of photinos and gluinos.

Keywords Models beyond the standard model · Supersymmetric model · Total cross section

1 Introduction

Supersymmetry (SUSY) was introduced more than 30 years ago, in independent theoretical papers by Gol'fand and Likhtman [1, 2], Volkov and Akulov [3], and Wess and Zumino [4–6]. In the first of these articles [1, 2], the authors found the superextension of the Poincaré algebra and constructed the first four-dimensional field theory with supersymmetry, the (massive) supersymmetric quantum electrodynamics (SQED).

The particle content of SQED is given by the electron (fermion), positron (antifermion), which are Dirac fermions [7, 8], the photon, and the spin-0 partners of the electron and the positron, the so-called selectron and spositron (sfermions). Also included in the model is the photino, the spin-$(1/2)$ superpartner of the photon. The photon and the photino are introduced in the same vector superfield, therefore the photino must be a Majorana fermion [9]. In this theory, both the R-parity and the chirality are conserved, and sparticles appear in pairs at any vertex (see [10–16]).

The history of the minimal supersymmetric standard model (MSSM), which was constructed in 1975 [17–20], can be found in Refs. [21, 22]. In the early days of the model, the photino, which is denoted by the symbol $\tilde{\gamma}$, was called the "photon–neutrino" and envisioned as a fundamental particle, expected to be stable [23] and, at least at the classical level, massless [24].

Within the context of supersymmetric field theories, two-component Weyl-van der Waerden fermions [25] enter naturally, due to the spinorial nature of the symmetry generators themselves and the holomorphic structure of the superpotential. Using the two-component spinors, we can introduce the helicity formalism, in which the individual amplitudes are computed analytically in terms of Lorentz scalar invariants, i.e., of complex numbers that can readily be computed. It is then a simple numerical task to sum all the

D. B. Espindola
Instituto de Física-IF-UFRGS,
Universidade Federal do Rio Grande do Sul,
Av. Bento Gonçalves, 9500,
Caixa Postal 15051, Cep:91501-970,
Porto Alegre, Rio Grande do Sul, Brazil

M. C. Rodriguez (✉) · C. B. Mariotto
Instituto de Matemática, Estatística e Física-IMEF,
Universidade Federal do Rio Grande-FURG,
Av. Itália, km 8, Campus Carreiros,
Caixa Postal 474, Cep:96200-970,
Rio Grande, Rio Grande do Sul, Brazil
e-mail: marcosrodriguez@furg.br

contributing amplitudes and compute the square of the complex magnitude of the resulting sum [26–28].[1]

As a simple example, consider Bhabha scattering $e^-e^+ \to e^-e^+$ [29] in QED. We denote the initial-state momenta and helicities of the electron and positron (p_1, λ_1) and (p_2, λ_2), respectively, and the final-state momenta and helicities of the electron and positron (p_3, λ_3) and (p_4, λ_4), respectively. In the formalism of four-component Dirac spinors, the amplitude for the s channel is given by the equality

$$\mathcal{M} = \frac{e^2}{s}\bar{u}(p_3,\lambda_3)\gamma^m v(p_4,\lambda_4)\bar{v}(p_2,\lambda_2)\gamma_m v(p_1,\lambda_1). \quad (1)$$

For the same process, in the two-spinor formalism, the amplitude is given by the following expression [26–28]:

$$\begin{aligned}\imath\mathcal{M} = \left(\frac{\imath g^{mn}}{s}\right)\Big[&\left(\imath e x_1\sigma_m y_2^\dagger\right)\left(-\imath e y_3\sigma_n x_4^\dagger\right) + \left(\imath e y_1^\dagger\bar{\sigma}_n x_2\right)\\ &\times\left(-\imath e y_3\sigma_n x_4^\dagger\right)+\left(\imath e x_1\sigma_m y_2^\dagger\right)\left(-\imath e x_3^\dagger\bar{\sigma}_n y_4\right)\\ &+\left(\imath e y_1^\dagger\bar{\sigma}_n x_2\right)\left(-\imath e x_3^\dagger\bar{\sigma}_n y_4\right)\Big]. \quad (2)\end{aligned}$$

For a more extensive discussion of this formalism and other useful examples, see Ref. [28].

Parity-conserving theories such as QED and QCD are well suited to the four-component fermion methods. The latter being more broadly known than the two-component methods, our discussion will be based on Majorana–(Dirac) four-component spinors.

Early in its history, the gluino, which is denoted $\tilde{g}$, was called the "photonic neutrino" and viewed as a massless particle, since it was difficult to generate a sizeable mass for it. The role and interactions of this fermion partner of the gluon, which, like the photino, is a Majorana fermion, are directly related to the properties of supersymmetric QCD (SQCD) [10, 11]. In the early days, the existence of relatively light "R-hadrons"[2] [30, 31] was therefore expected. Today, we know that a direct gaugino mass, symbolized $m_{1/2}$, comes from supergravity [32], or from radiative corrections using messenger quarks. Both mechanisms yield sufficiently high masses for the gluino.

The phenomenological studies of the photinos started in 1979, when Fayet [24] studied the interaction between photinos[3] and matter for massless photinos and obtained the following cross section:

$$\sigma\left(\tilde{\gamma}+e^-\to\tilde{\gamma}+e^-\right) = \frac{4G_F^2 m_e E}{6\pi}\left(\frac{4M_W^2\sin^2\theta_W}{m_{s_e}^2}\right)^2, \quad (3)$$

where m_{s_e} is the mass of the slepton. See Ref. [22] for the early notation.

Later, in 1982, Fayet [33] studied the photino production from e^-e^+, still in the case of massless photinos, with the following result:

$$\begin{aligned}&\frac{\mathrm{d}\sigma}{\mathrm{d}\Omega}(e^-e^+\to\tilde{\gamma}\tilde{\gamma})\\ &=\frac{\alpha^2 s}{16}\left[\frac{(1-\cos^2\theta)^2}{\left(m_{s_e}^2+\frac{s}{2}(1-\cos^2\theta)\right)^2}+\frac{(1+\cos^2\theta)^2}{\left(m_{t_e}^2+\frac{s}{2}(1+\cos^2\theta)\right)^2}\right], \quad (4)\end{aligned}$$

where θ is the angle between the photino and the incoming electron, and s is the usual Mandelstam variable.

A later computation considered a massive photino [34, 35]. The mass $m_{\tilde{\gamma}}$ acquired phenomenological importance because it was related to the scale of supersymmetry breaking [23], to which, more recently, the mass of the gluino has also been related. With a massive photino, the total cross section is [33]

$$\sigma\left(e^-e^+\to\tilde{\gamma}\tilde{\gamma}\right) = \frac{2\pi\alpha^2 s}{3m_{s_e}^4}. \quad (5)$$

Fayet also analyzed the processes $e^-e^+\to\gamma\nu\bar{\nu}$ and $e^-e^+\to\gamma\tilde{\gamma}\tilde{\gamma}$ to obtain the following total cross sections (in pb) [33]:

$$\begin{aligned}&\sigma\left(e^-e^+\to\gamma\nu\bar{\nu}\right)\approx 2.6\cdot 10^{-2}\frac{s}{(40\mathrm{GeV})^2},\\ &\sigma\left(e^-e^+\to\gamma\tilde{\gamma}\tilde{\gamma}\right) = 18\left(\frac{m_{s_e}}{40\frac{\mathrm{GeV}}{c^2}}\right)^{-4}\frac{s}{(40\mathrm{GeV})^2}. \quad (6)\end{aligned}$$

Only in 1984 were the photino and selectron masses included in these processes [36–38]. At the time, it was thought that these reactions might define a useful signature of SUSY and the experiments, important limits on the photino and selectron masses. Two years later, the reactions $e^-e^+\to\gamma\nu\bar{\nu}$ and $e^-e^+\to\gamma\tilde{\gamma}\tilde{\gamma}$ were accurately analyzed, and the results showed that the

[1] Reference [28] discusses the history of the spinors and the techniques in the two-component spinor formalism and provides a complete set of Feynman rules for fermions in two-component spinor notation.

[2] Particle made of quarks, antiquarks, and gluinos.

[3] In the MSSM context, the photino interacts more weakly than the neutrino.

latter process has larger cross section than the former (see Fig. 2 in Ref. [38]), a finding applicable only to the "lower" selectron masses. It was also found that the processes with polarized and unpolarized beams place strong limits on the $m_{\tilde{\gamma}} \times m_{\tilde{e}}$ plane (see Fig. 4 in Ref. [38]) [39]. A photino production in this channel was analyzed in detail in Ref. [40].

Low-mass weakly interacting particles (photinos, neutrinos, axions, etc.) are produced in hot astrophysical plasmas and can therefore transport energy out of stars. The possible astrophysical consequences of "light" photinos and gluinos, for which the main photino production channel is the subprocess $gg \to \tilde{g}\tilde{g}$ followed by a gluino decay $\tilde{g} \to \tilde{\gamma}\bar{q}q$, were discussed in Refs. [23, 41].

It has been generally assumed that, for small gaugino masses, the photino is an approximate eigenstate, an assumption that is not generally valid. The classic signature of such events is missing transverse momentum ($\not{p}_T$) from the escaping photinos. The analysis of the UA1 Collaboration gave special attention to this characteristic [42].

Unfortunately, the data analyses of the large electron positron collider at the CERN (LEP) were unable to follow the same approach. For larger gaugino masses, it is unproductive to think in terms of the photino, zino, and neutrals higgsinos ($\tilde{h}_1^0$ and $\tilde{h}_2^0$). Instead, one must consider the mixture of these states giving four neutralinos $\tilde{\chi}_j^0$, $j = 1, 2, 3, 4$. In a similar way, the mixing of the charged gauginos with the charged higgsinos gives two charginos $\tilde{\chi}_i^{\pm}$, $i = 1, 2$. The dominant gluino decays then occur via $\tilde{g} \to \tilde{q}_i q_j \tilde{\chi}_k^{\pm}$ and $\tilde{g} \to \bar{q}q\tilde{\chi}_i^0$ [11, 14, 42, 43].

The rate of the two-body decay $\tilde{g} \to \tilde{\gamma}g$ of the gluinos was first analyzed in Ref. [44], where this decay rate was found to vanish for $m_{\tilde{q}_L} = m_{\tilde{q}_R}$. The partial width for the gluino radiative decay was recomputed (for $m_{\tilde{\gamma}} = 0$) in Refs. [45, 46]. The most general result for the radiative decay width of the gluinos was obtained in Ref. [44] for the photino as the lightest supersymmetric particle (LSP) [43]. Only with very massive gluinos ($m_{\tilde{g}} > (m_q + m_{\tilde{q}})$) do the two-body decays into quark plus squark become kinematically accessible and rapidly dominate the branching fraction [11, 14].

Notwithstanding the appealing arguments favoring SUSY, no supersymmetric particle has been found so far, in the first large hadron collider (LHC) runs of up to 8 TeV CM energies [47–49]. With the increasing luminosity and energies up to 14 TeV in the next years, however, the prospect for discoveries is still good. The search is aided by the "snowmass points and slopes" (SPS) [50], a set of benchmark points and parameter lines in the MSSM parameter space corresponding to different scenarios in the quest for supersymmetry (see Ref. [51] for an instructive review). The goal here is to reconstruct the fundamental supersymmetric theory, and its breaking mechanism, from the experimental data [50–52]. Therefore, in various scenarios, given the SPS convention, the neutralinos (photinos) are the lighter particles, while the gluino is the most massive particle of the MSSM. As indicated in Table 1, each set of parameters leads to different masses for the gluinos, squarks, photinos, and selectrons, which are the only relevant parameters in the study.

Table 1 Masses of gluinos, squarks, photinos, and selectrons in the SPS scenarios

Scenario	$m_{\tilde{g}}$ (GeV)	$M_{\tilde{q}}$ (GeV)	$m_{\tilde{\gamma}}$ (GeV)	$M_{\tilde{e}}$ (GeV)
SPS1a	595.2	539.9	96	202
SPS1b	916.1	836.2	96	202
SPS2	784.4	1,533.6	79	1,456
SPS3	914.3	818.3	160	287
SPS4	721.0	732.2	118	448
SPS5	710.3	643.9	119	256
SPS6	708.5	641.3	189	264
SPS7	926.0	861.3	161	261
SPS8	820.5	1,081.6	137	356
SPS9	1,275.2	1,219.2	175	319

Supersymmetric theories involve self-conjugate Majorana spinors. In Section 2, we review the prescription for writing Feynman rules for Majorana particles, which are based on a well-defined fermion flow, a procedure that is similar to the one leading to Feynman amplitudes for Dirac fermions. Sections 3 and 4, which detail the calculation of the differential cross section for the production of photinos and gluinos, respectively, are followed by conclusions.

2 Feynman Rules for Majorana Particles

Neutral particles may or may not have distinct antiparticles. While Dirac fermions [7, 8] have distinct antiparticles, the neutron being an example, the contrary is true for Majorana fermions [9], the field operators of which therefore satisfy the equalities[4] [34]

$$\psi_M = \psi_M^c \equiv C\bar{\psi}_M^T,$$
$$\bar{\psi}_M = \psi_M^T C, \tag{7}$$

[4] Appendix D of Ref. [34] discusses this subject in detail.

where $\bar{\psi} \equiv \psi^\dagger \gamma^0$, while C is the charge conjugation matrix. The latter has the following properties

$$\begin{aligned} &C^\dagger = C^{-1}, \ \ C^T = -C, \\ &C^{-1}\Gamma_i C = \Gamma_i^T, \ \text{ for } \Gamma_i = I_{4\times4}, \imath\gamma_5, \gamma_m\gamma_5, \\ &C^{-1}\Gamma_i C = -\Gamma_i^T, \ \text{ for } \Gamma_i = \gamma_m, \sigma_{m,n} = \frac{\imath}{2}[\gamma_m, \gamma_n]. \end{aligned} \tag{8}$$

The Γ_i have been chosen such that

$$\Gamma_i^\dagger = \eta_i \gamma^0 \Gamma_i \gamma^0, \tag{9}$$

with no summation over i, where η_i is defined as

$$\eta_i = \begin{cases} 1 \ \text{ for } i = I_{4\times4}, i\gamma_5, \gamma_m, \\ -1 \text{ for } i = \ \ \gamma_m, \sigma_{m,n}\,. \end{cases} \tag{10}$$

In general, the u and v spinors for either Dirac or Majorana fermions are related by the equalities

$$\begin{aligned} &u^c \equiv C\bar{u}^T = v, \ \ \bar{u}^{(s)T} = C^{-1}v^{(s)}, \ \ v^{(s)T} = \bar{u}^{(s)}C^T, \\ &v^c \equiv C\bar{v}^T = u, \ \ \bar{v}^{(s)T} = C^{-1}u^{(s)}, \ \ u^{(s)T} = \bar{v}^{(s)}C^T, \end{aligned} \tag{11}$$

where $s = \pm 1/2$ labels the spin.

The Feynman rules for Majorana fermions, in contrast with those for Dirac fermions, involve vertices and propagators with clashing arrows. As a consequence, charge–conjugation matrices appear in the Feynman rules for vertices and propagators, as discussed in Refs. [11, 14, 15, 34].

2.1 Problems in Defining Feynman Rules for a Majorana Field

In the standard model (SM) [53, 54], all the interactions conserve both the Baryon number (B) and the Lepton number (L). By contrast, the MSSM [17–20, 34] comprises interactions that violate the conservation of fermion number, because the Majorana fermions lack distinct antiparticles. Their self-conjugacy allows a variety of different contractions, which acquire different signs due to the anticommutation of fermionic operators [34, 55, 56].

The usual Dirac field spinor expansion is given by the expression [14]

$$\Psi_D(x) = \int \frac{\mathrm{d}^3k}{(2\pi)^3}\frac{1}{2E_{\vec{k}}} \sum_{s=\mp1/2} \times \left[c_{\vec{k},s}u^{(s)}(k)e^{-ikx} + d^\dagger_{\vec{k},s}v^{(s)}(k)e^{ikx}\right], \tag{12}$$

where $c(c^\dagger)$ and $d(d^\dagger)$ are annihilation (creation) operators satisfying

$$\begin{aligned} &\left[c_{\vec{k},s}, c^\dagger_{\vec{l},r}\right] = (2\pi)^3 2E_{\vec{k}}\delta_{sr}\delta^3\left(\vec{k}-\vec{l}\right), \\ &\left[c_{\vec{k},s}, c_{\vec{l},r}\right] = \left[c^\dagger_{\vec{k},s}, c^\dagger_{\vec{l},r}\right] = 0, \\ &\left[d_{\vec{k},s}, d^\dagger_{\vec{l},r}\right] = (2\pi)^3 2E_{\vec{k}}\delta_{sr}\delta^3\left(\vec{k}-\vec{l}\right), \\ &\left[d_{\vec{k},s}, d_{\vec{l},r}\right] = \left[d^\dagger_{\vec{k},s}, d^\dagger_{\vec{l},r}\right] = 0. \end{aligned} \tag{13}$$

To quantize the Dirac spinor field Ψ_D, one requires that

$$\begin{aligned} &\{\Psi_{Da}(x), \Psi^\dagger_{Db}(y)\} = \delta_{ab}\delta^3(\vec{x}-\vec{y}), \\ &\{\Psi_{Da}(x), \Psi_{Db}(y)\} = \{\Psi^\dagger_{Da}(x), \Psi^\dagger_{Db}(y)\} = 0. \end{aligned} \tag{14}$$

For a Dirac spinor, therefore, we can write the following expressions:

$$\begin{aligned} &\langle 0|T\left\{\Psi_{Da}(x)\bar{\Psi}_{Db}(y)\right\}|0\rangle = S_{Fab}(x-y), \\ &\langle 0|T\{\Psi_{Da}(x)\Psi_{Db}(y)\}|0\rangle = \langle 0|T\left\{\bar{\Psi}_{Da}(x)\bar{\Psi}_{Db}(y)\right\}|0\rangle = 0. \end{aligned} \tag{15}$$

We represent a fermion in a Feynman diagram by a solid line. For a Dirac fermion, each line carries an arrow indicating the fermion number flow.

The analogous expressions for the Majorana fermions [14] are

$$\begin{aligned} \Psi_M(x) &= \int \frac{\mathrm{d}^3k}{(2\pi)^3}\frac{1}{2E_{\vec{k}}} \\ &\quad\times \sum_{s=\mp1/2}\left[c_{\vec{k},s}u^{(s)}(k)e^{-ikx} + c^\dagger_{\vec{k},s}v^{(s)}(k)e^{ikx}\right], \\ \left[c_{\vec{k},s}, c^\dagger_{\vec{l},r}\right] &= (2\pi)^3 2E_{\vec{k}}\delta_{sr}\delta^3\left(\vec{k}-\vec{l}\right), \\ \left[c_{\vec{k},s}, c_{\vec{l},r}\right] &= \left[c^\dagger_{\vec{k},s}, c^\dagger_{\vec{l},r}\right] = 0, \\ \langle 0|T\left\{\Psi_{Ma}(x)\bar{\Psi}_{Mb}(y)\right\}|0\rangle &= S_{Fab}(x-y), \\ \langle 0|T\{\Psi_{Ma}(x)\Psi_{Mb}(y)\}|0\rangle &= \langle 0|T\left\{\Psi_{Ma}(x)\bar{\Psi}_{Mc}(y)\right\}|0\rangle C^T_{cb} \\ &= S_{Fac}(x-y)C^T_{cb}, \\ \langle 0|T\left\{\bar{\Psi}_{Ma}(x)\bar{\Psi}_{Mb}(y)\right\}|0\rangle &= C^T_{ac}\langle 0|T\left\{\Psi_{Mc}(x)\bar{\Psi}_{Mb}(y)\right\}|0\rangle \\ &= C^T_{ac}S_{Fcb}(x-y), \end{aligned} \tag{16}$$

where c and $c^\dagger$ are annihilation and creation operators,[5] and we have to include these contractions to compute matrix elements of operators involving products of

[5] The condition $c_{\vec{k},s} = d_{\vec{k},s}$ implies the identity of the particle and antiparticle quanta of this field.

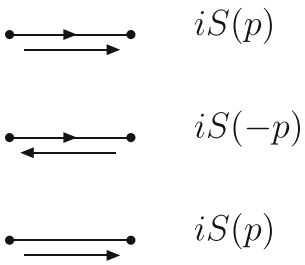

Fig. 1 Feynman rules for an internal Dirac fermion line. For each diagram, the *upper line* represents the fermion momentum, and the *lower line* represents the fermion flow

Majorana spinor fields [14, 34]. In contrast with Dirac lines, Majorana lines carry no arrows.

For Dirac fields, the internal propagator reads

$$\langle 0|T\left\{\Psi(x)\bar{\Psi}(y)\right\}|0\rangle \to \frac{1}{\not{P}-m} = S(P), \tag{17}$$

where the propagating fields Ψ carries a momentum P.

The contraction with the external operators is given by the expressions [55, 56]

$$\begin{aligned}
\langle 0|T\left\{\Psi(x)c^{\dagger}(p_i,s_i)\right\}|0\rangle &\to u(p_i,s_i),\\
\langle 0|T\left\{c(p_i,s_i)\bar{\Psi}(x)\right\}|0\rangle &\to \bar{u}(p_i,s_i),\\
\langle 0|T\left\{\Psi(x)d^{\dagger}(p_i,s_i)\right\}|0\rangle &\to \bar{v}(p_i,s_i),\\
\langle 0|T\left\{d(p_i,s_i)\bar{\Psi}(x)\right\}|0\rangle &\to v(p_i,s_i).
\end{aligned} \tag{18}$$

In general, each Dirac field is associated with the usual propagator $S(P)$ (see (17)), and the "reversed" one $S(-P)$, as drawn in Fig. 1, as well as with the usual spinors and their "reversed" counterparts, given by (18), which are depicted in Fig. 2. For Majorana fermions, since arrows cannot be drawn to indicate the fermion number flow, we only have the usual propagator $S(P)$ and spinors, not the reversed ones, as shown by Fig. 3. Notice that the propagator has clashing arrows [55, 56].

The most generic Lagrangian $\mathcal{L}$ for Majorana fields λ and Dirac fields ψ [34], augmented by a pure Dirac

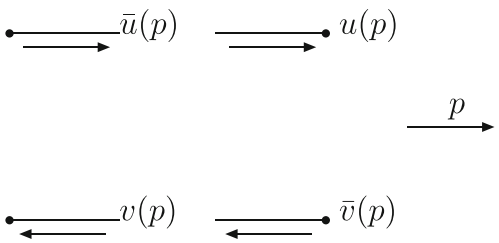

Fig. 2 Feynman rules for an external Dirac fermion line. The momentum p flows from the left to the right

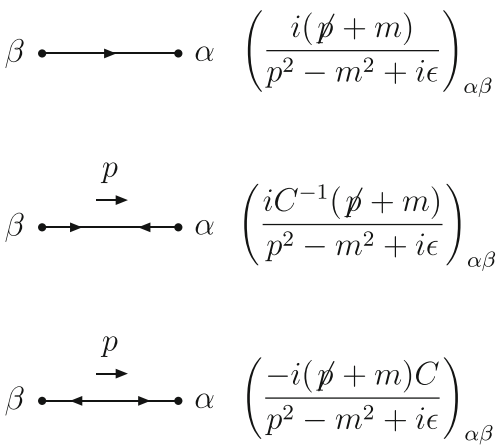

Fig. 3 Feynman rules for Majorana fermion propagators with orientation (*thin arrows*). The momentum p flows from left to right

interaction term [55, 56], can be expressed by the following expression:

$$\begin{aligned}
\mathcal{L} = {} & \frac{1}{2}\bar{\lambda}_a\left(\imath\gamma^m\partial_m - M_a\right)\lambda_a + \bar{\psi}_a\left(\imath\gamma^m\partial_m - m_a\right)\psi_a\\
& + \frac{1}{2}g^i_{abc}\bar{\lambda}_a\Gamma_i\lambda_b\,\Phi_c + \frac{1}{2}g^{i*}_{abc}\bar{\lambda}_b\,\Gamma_i\lambda_a\Phi^*_c\\
& + \kappa^i_{abc}\bar{\lambda}_a\Gamma_i\psi_b\,\Phi^*_c + \kappa^{i*}_{abc}\bar{\psi}_b\,\Gamma_i\lambda_a\Phi_c + h^i_{abc}\bar{\psi}_a\Gamma_i\psi_b\,\Phi_c,
\end{aligned} \tag{19}$$

where Γ_i is defined in (8), and g^i_{abv}, κ^i_{abc} and h^i_{abc} are coupling constants.

The field Φ summarizes scalar and vector fields. Using (8) and the fact that fermion fields anticommute in the first term on the second line, we find that the following constraint must be satisfied:

$$g^i_{abc} = \eta_i g^i_{bac}\,, \tag{20}$$

with no summation over i and η given by (10).

The second problem, as shown in Ref. [34], is the following. The two terms on the second line of (19) can be rewritten as

$$\begin{aligned}
g^i_{abc}\bar{\lambda}_a\Gamma_i\lambda_b\,\Phi_c &= -g^i_{abc}\bar{\lambda}^T_a\left(C^{-1}\Gamma_i\right)\lambda_b\,\Phi_c,\\
g^{i*}_{abc}\bar{\lambda}_b\,\Gamma_i\lambda_a\Phi^*_c &= g^{i*}_{abc}\bar{\lambda}_b\,\left(\Gamma_i C\right)\bar{\lambda}^T_a\Phi^*_c,
\end{aligned} \tag{21}$$

and hence the Feynman rules for this term may then be given by any of the following conventions:

$$\begin{aligned}
ig^i_{abc}\Gamma &= -ig^i_{abc}\left(C^{-1}\Gamma_i\right),\\
ig^{i*}_{abc}\Gamma &= ig^{i*}_{abc}\left(\Gamma C\right),
\end{aligned} \tag{22}$$

which seem to give evidence of sign ambiguity.

Another problem derives from the location of the C operator [34]. The self-conjugacy allows for a variety

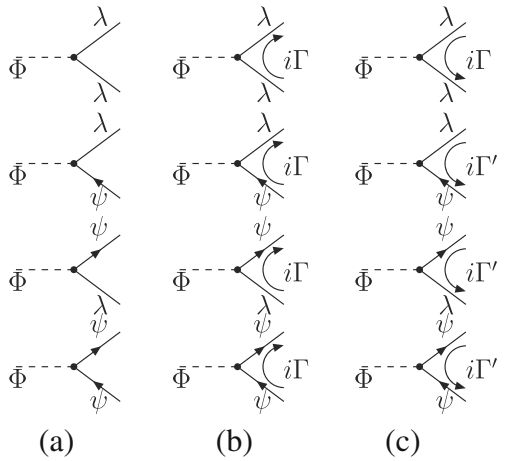

Fig. 4 Feynman rules for the interaction (from (19)) of a scalar field with one Majorana (λ) fermion. From Refs. [55, 56]

of different contractions, which acquire different signs originating from the anticommutation of fermionic operators [34, 55, 56]. In this approach, the relative sign of interfering Feynman graphs cannot be read off the graphs but has to be determined independently from the Wick contractions. This method is unwieldy in such practical calculations as the production of photinos and gluinos.

There is, however, an alternative way to define Feynman rules for Majorana fermions. Since the fermion-flow rule is violated, we may introduce a continuous fermion-flow orientation for each fermion line, as in Refs. [55–57].[6] This forces us to introduce two analytical expressions for each vertex, one for fermion flow parallel and the other for fermion flow antiparallel to the flow of the fermion number. Therefore, for Majorana fermions, only the usual spinors are present, as in Fig. 4.

The Feynman amplitudes can be obtained from the following procedure [55, 56]:

1. Draw all possible Feynman diagrams for a given process;
2. Fix an arbitrary orientation (fermion flow) for each fermion chain;
3. Start at an external leg (for closed loops at some arbitrary propagator) and write down the Dirac matrices proceeding opposite to the chosen orientation (fermion flow) through the chain in agreement with Fig. 2;
4. Apply the corresponding analytical expressions;
5. Multiply by a factor (-1) for every closed loop;
6. Multiply by the permutation parity of the spinors in the obtained analytical expression with the respect to some reference order;
7. As far as determining the combinatorial factor is concerned, Majorana fermions behave exactly like real scalar or vector fields.

We can understand the last item in the following way: for Majorana fermions, there are two equivalent nonvanishing Wick contractions, i.e.,

$$\bar{\chi}\Gamma\chi = \overline{\tilde{\chi}}\Gamma'\tilde{\chi}. \tag{23}$$

For Majorana fermions $\tilde{\chi} = \chi$, an equality that, together with (20), allows us to show that

$$\Gamma' = \Gamma. \tag{24}$$

These two contractions yield the same result and cancel the factor $1/2$ in the corresponding interaction term. This is exactly what happens for real scalar and vectors fields. The analytical expressions are independent of the chosen orientation, i.e., of the fermion flow, as shown by Refs. [55, 56].

This set of rules, which will be shown in the next sections to simplify practical calculations, can be combined with the FeynArts program [58] to calculate the differential cross sections for photino and gluino production.

In general, to calculate the square amplitudes involving Dirac fermions, we use the following projection operators in diagrams involving Majorana fermions, which are obtained from (11):

$$\begin{aligned}
\sum_s u^{(s)}(P)v^{(s)T}(P) &= \left(\sum_s u^{(s)}(P)\bar{u}^{(s)}(P)\right)C^T \\
&= (\not{P} + M)C^T, \\
\sum_s v^{(s)}(P)u^{(s)T}(P) &= \left(\sum_s v^{(s)}(P)\bar{v}^{(s)}(P)\right)C^T \\
&= (\not{P} - M)C^T, \\
\sum_s \bar{u}^{(s)T}(P)\bar{v}^{(s)}(P) &= C^{-1}\left(\sum_s v^{(s)}(P)\bar{v}^{(s)}(P)\right) \\
&= C^{-1}(\not{P} - M), \\
\sum_s \bar{v}^{(s)T}(P)\bar{u}^{(s)}(P) &= C^{-1}\left(\sum_s u^{(s)}(P)\bar{u}^{(s)}(P)\right) \\
&= C^{-1}(\not{P} + M),
\end{aligned} \tag{25}$$

where C is the charge conjugation matrix satisfying (8).

[6] We only need the familiar Dirac propagator and only vertices without explicit charge–conjugation matrices.

3 Photino Production

This section shows how to calculate the differential cross section of the $e^-e^+ \to \tilde{\gamma}\tilde{\gamma}$ process, where $\tilde{\gamma}$ is the photino field in the SQED context. This process, which conserves the lepton number, takes place via t-channel $\tilde{e}_L^-$- and $\tilde{e}_R^-$-exchange (see Fig. 5) as shown by Fayet [33]. We will assume that $\tilde{e}_L^-$- and $\tilde{e}_R^-$ are mass eigenstates, because we are in the domain of SQED. Both e and $\tilde{e}$ carry one unit of lepton number. The t- and u-channel exchanges correspond to the cases where the fermion lines are uncrossed and crossed, respectively.

Today, we know that in the context of the MSSM, the photino is a gaugino and mixes with the neutral higgsinos to yield the neutralinos as the mass eigenstates [11, 14, 59]. Neutralino pair production in e^-e^+ collisions was first studied in [60], where it was shown that this production takes place via the s-channel Z-exchange and t-channel $\tilde{e}_L^-$- and $\tilde{e}_R^-$-exchange. On the other hand, the LSP in some minimal Supergravity (mSUGRA) scenarios can be a light photino, i.e., $\tilde{\chi}_1^0 \approx \tilde{\gamma}$ [50–52], with an acceptable cosmological abundance [61].

In e^-e^+ collisions, photinos are produced in the following reaction:

$$e^-(P_1) + e^+(P_2) \to \tilde{\gamma}(K_1) + \tilde{\gamma}(K_2) \tag{26}$$

as shown in Fig. 5, where $\tilde{\gamma}$ is the photino, and the particle four-momenta are specified in parentheses. As already explained, the photino is its own antiparticle.

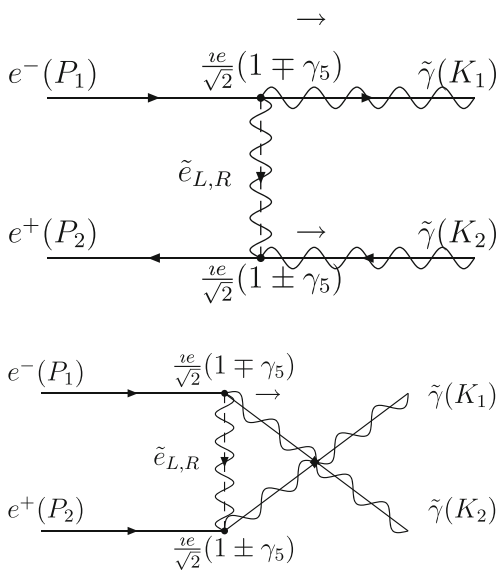

Fig. 5 Feynman diagram of the process $e^-e^+ \to \tilde{\gamma}\tilde{\gamma}$. The electron fixes the orientation (fermion flow) for each lepton. The positron line has, therefore, the opposite direction, and a continuous line results in the diagram

The amplitudes for $e^-(P_1)e^+(P_2) \to \tilde{\gamma}(K_1)\tilde{\gamma}(K_2)$ are

$$\begin{aligned}
\mathcal{M}_a &= -\frac{e^2}{2}\bar{u}(K_1)(1-\gamma_5)u(P_1)\frac{1}{t-M_{\tilde{e}_L}^2}\bar{v}(P_2) \\
&\quad \times (1+\gamma_5)v(K_2), \\
\mathcal{M}_b &= \frac{e^2}{2}\bar{u}(K_1)(1+\gamma_5)u(P_1)\frac{1}{t-M_{\tilde{e}_R}^2}\bar{v}(P_2) \\
&\quad \times (1-\gamma_5)v(K_2), \\
\mathcal{M}_c &= -\frac{e^2}{2}\bar{u}(K_2)(1-\gamma_5)u(P_1)\frac{1}{u-M_{\tilde{e}_L}^2}\bar{v}(P_2) \\
&\quad \times (1+\gamma_5)v(K_1), \\
\mathcal{M}_d &= \frac{e^2}{2}\bar{u}(K_2)(1+\gamma_5)u(P_1)\frac{1}{u-M_{\tilde{e}_R}^2}\bar{v}(P_2) \\
&\quad \times (1-\gamma_5)v(K_1),
\end{aligned} \tag{27}$$

where s, t, u are the Mandelstam variables, defined as

$$\begin{aligned}
s &= (P_1+P_2)^2 = (K_1+K_2)^2, \\
t &= (P_1-K_1)^2 = (P_2-K_2)^2, \\
u &= (P_1-K_2)^2 = (P_2-K_1)^2, \\
s+t+u &= 2m_e^2 + 2m_{\tilde{\gamma}}^2.
\end{aligned} \tag{28}$$

Here, m_e and $m_{\tilde{\gamma}}$ are the electron and the photino masses, respectively.

The next step is to calculate $|\mathcal{M}_a + \mathcal{M}_b + \mathcal{M}_c + \mathcal{M}_d|^2$, where the relative negative signs, explicitly shown in Eq. (27), are due to the Pauli statistics. Summing over initial and final spins and using the usual projection operator over the positive and negative energy states, we obtain (see Ref. [66] for more details on the algebraic manipulations) the following expressions:

$$\begin{aligned}
|\mathcal{M}_a|^2 &= \frac{16e^4}{(t-M_{\tilde{e}_L}^2)^2}(P_1\cdot K_1)(P_2\cdot K_2) \\
&= \frac{4e^4}{(t-M_{\tilde{e}_L}^2)^2}\left(t-m_e^2-m_{\tilde{\gamma}}^2\right)^2, \\
\mathcal{M}_a^\dagger\mathcal{M}_b &= \mathcal{M}_b\mathcal{M}_a^\dagger = \frac{e^4}{4(t-M_{\tilde{e}_L}^2)(t-M_{\tilde{e}_R}^2)}(8m_e m_{\tilde{\gamma}})^2, \\
|\mathcal{M}_b|^2 &= \frac{16e^4}{(t-M_{\tilde{e}_R}^2)^2}(P_1\cdot K_1)(P_2\cdot K_2) \\
&= \frac{4e^4}{(t-M_{\tilde{e}_R}^2)^2}\left(t-m_e^2-m_{\tilde{\gamma}}^2\right)^2,
\end{aligned}$$

$$|\mathcal{M}_c|^2 = \frac{16e^4}{(u-M_{\tilde{e}_L}^2)^2}(P_1\cdot K_2)(P_2\cdot K_1)$$
$$= \frac{4e^4}{(u-M_{\tilde{e}_L}^2)^2}(u-m_e^2-m_{\tilde{\gamma}}^2)^2,$$
$$\mathcal{M}_c^\dagger\mathcal{M}_d = \mathcal{M}_d^\dagger\mathcal{M}_c = \frac{e^4}{4(u-M_{\tilde{e}_R}^2)(u-M_{\tilde{e}_L}^2)}(8m_em_{\tilde{\gamma}})^2,$$
$$|\mathcal{M}_d|^2 = \frac{16e^4}{(u-M_{\tilde{e}_R}^2)^2}(P_1\cdot K_2)(P_2\cdot K_1)$$
$$= \frac{4e^4}{(u-M_{\tilde{e}_R}^2)^2}(u-m_e^2-m_{\tilde{\gamma}}^2)^2. \tag{29}$$

Let us work out the interference terms in detail. On this case, we need again to sum over initial and final spins. From (25), we find that

$$\mathcal{M}_a^\dagger\mathcal{M}_c = \mathcal{M}_c^\dagger\mathcal{M}_a = \frac{e^4}{4(u-M_{\tilde{e}_L}^2)(t-M_{\tilde{e}_L}^2)}$$
$$\cdot\left\{\mathrm{Tr}\left[(1-\gamma_5)(\not{P}_1+m_e)(1+\gamma_5)\right.\right.$$
$$\cdot(\not{K}_1+m_{\tilde{\gamma}})C^T(1+\gamma_5)^T(\not{P}_2-m_e)^T$$
$$\left.\left.\cdot\ (1-\gamma_5)^TC^{-1}(\not{K}_2+m_{\tilde{\gamma}})\right]\right\},$$
$$\mathcal{M}_a^\dagger\mathcal{M}_d = \mathcal{M}_d^\dagger\mathcal{M}_a = \frac{e^4}{4(t-M_{\tilde{e}_L}^2)(u-M_{\tilde{e}_R}^2)}$$
$$\cdot\left\{\mathrm{Tr}\left[(1+\gamma_5)(\not{P}_1+m_e)(1+\gamma_5)\right.\right.$$
$$\cdot(\not{K}_1+m_{\tilde{\gamma}})C^T(1-\gamma_5)^T(\not{P}_2-m_e)^T$$
$$\left.\left.\cdot\ (1+\gamma_5)^TC^{-1}(\not{K}_2+m_{\tilde{\gamma}})\right]\right\},$$
$$\mathcal{M}_b^\dagger\mathcal{M}_c = \mathcal{M}_c^\dagger\mathcal{M}_b = \frac{e^4}{4(t-M_{\tilde{e}_L}^2)(u-M_{\tilde{e}_R}^2)}$$
$$\cdot\left\{\mathrm{Tr}\left[(1-\gamma_5)(\not{P}_1+m_e)(1+\gamma_5)\right.\right.$$
$$\cdot(\not{K}_1+m_{\tilde{\gamma}})C^T(1-\gamma_5)^T(\not{P}_2-m_e)^T$$
$$\left.\left.\cdot\ (1-\gamma_5)^TC^{-1}(\not{K}_2+m_{\tilde{\gamma}})\right]\right\},$$
$$\mathcal{M}_b^\dagger\mathcal{M}_d = \mathcal{M}_d^\dagger\mathcal{M}_b = \frac{e^4}{4(u-M_{\tilde{e}_R}^2)(t-M_{\tilde{e}_R}^2)}$$
$$\cdot\left\{\mathrm{Tr}\left[(1+\gamma_5)(\not{P}_1+m_e)(1-\gamma_5)\right.\right.$$
$$\cdot(\not{K}_1+m_{\tilde{\gamma}})C^T(1-\gamma_5)^T(\not{P}_2-m_e)^T$$
$$\left.\left.\cdot\ (1+\gamma_5)^TC^{-1}(\not{K}_2+m_{\tilde{\gamma}})\right]\right\}. \tag{30}$$

We now need to calculate the quantity

$$C^T(1+\gamma_5)^T(\not{P}_2-m_e)^T(1-\gamma_5)^TC^{-1}. \tag{31}$$

Notice taken that $[C,\gamma_5]=0$ and $\gamma_5^T=\gamma_5$, with the first two equalities in (8), we can show that

$$C^T(1+\gamma_5)^T = (1^T-\gamma_5^T)C^T = -(1-\gamma_5)C,$$
$$(1-\gamma_5)^TC^{-1} = C^T(1^T+\gamma_5^T) = C^{-1}(1+\gamma_5), \tag{32}$$

and using the last equality in (8), we can rewrite (31) in the form

$$-(1-\gamma_5)(P_2^mC\gamma_m^TC^{-1}-m_eCC^{-1})(1+\gamma_5)$$
$$= -(1-\gamma_5)(-P_2^m\gamma_m-m_e)(1+\gamma_5)$$
$$= (1-\gamma_5)(\not{P}_2+m_e)(1+\gamma_5). \tag{33}$$

We have, therefore, shown the following relation to hold:

$$C^T(1+\gamma_5)^T(\not{P}_2-m_e)^T(1-\gamma_5)^TC^{-1}$$
$$= (1-\gamma_5)(\not{P}_2+m_e)(1+\gamma_5). \tag{34}$$

Similarly, we can show that

$$C^T(1-\gamma_5)^T(\not{P}_2-m_e)^T(1+\gamma_5)^TC^{-1}$$
$$= (1+\gamma_5)(\not{P}_2+m_e)(1-\gamma_5). \tag{35}$$

Next, using the trace techniques, we find that

$$\mathcal{M}_a^\dagger\mathcal{M}_c = \mathcal{M}_c^\dagger\mathcal{M}_a = \frac{8e^4m_{\tilde{\gamma}}^2}{(u-M_{\tilde{e}_L}^2)(t-M_{\tilde{e}_L}^2)}(P_1\cdot P_2)$$
$$= \frac{8e^4m_{\tilde{\gamma}}^2}{(u-M_{\tilde{e}_L}^2)(t-M_{\tilde{e}_L}^2)}\left(\frac{s}{2}-m_e^2\right),$$
$$\mathcal{M}_a^\dagger\mathcal{M}_d = \mathcal{M}_d^\dagger\mathcal{M}_a = \frac{e^4}{4(t-M_{\tilde{e}_L}^2)(u-M_{\tilde{e}_R}^2)}(8m_em_{\tilde{\gamma}})^2,$$
$$\mathcal{M}_b^\dagger\mathcal{M}_c = \mathcal{M}_c^\dagger\mathcal{M}_b = \frac{e^4}{4(t-M_{\tilde{e}_R}^2)(u-M_{\tilde{e}_L}^2)}(8m_em_{\tilde{\gamma}})^2,$$
$$\mathcal{M}_b^\dagger\mathcal{M}_d = \mathcal{M}_d^\dagger\mathcal{M}_b = \frac{8e^4m_{\tilde{\gamma}}^2}{(u-M_{\tilde{e}_R}^2)(t-M_{\tilde{e}_R}^2)}(P_1\cdot P_2)$$
$$= \frac{8e^4m_{\tilde{\gamma}}^2}{(u-M_{\tilde{e}_R}^2)(t-M_{\tilde{e}_R}^2)}\left(\frac{s}{2}-m_e^2\right). \tag{36}$$

The differential cross section in the $M_{\tilde{e}_L} = M_{\tilde{e}_R} = M_{\tilde{e}}$ limit is then given by the relation

$$\frac{\mathrm{d}\sigma}{\mathrm{d}\Omega}(e^-e^+ \to \tilde{\gamma}\tilde{\gamma}) = \frac{\alpha^2}{4s}\sqrt{\frac{s-4m_{\tilde{\gamma}}^2}{s-4m_e^2}}\left[\left(\frac{t-m_{\tilde{\gamma}}^2-m_e^2}{t-M_{\tilde{e}}^2}\right)^2 + \left(\frac{u-m_{\tilde{\gamma}}^2-m_e^2}{u-M_{\tilde{e}}^2}\right)^2 + \left(\frac{2m_e m_{\tilde{\gamma}}}{t-M_{\tilde{e}}^2}\right)^2 + \left(\frac{2m_e m_{\tilde{\gamma}}}{u-M_{\tilde{e}}^2}\right)^2 + \left(\frac{16m_e^2m_{\tilde{\gamma}}^2 - 2sm_{\tilde{\gamma}}^2}{(t-M_{\tilde{e}}^2)(u-M_{\tilde{e}}^2)}\right)\right]. \quad (37)$$

Since the photino is not actually a mass eigenstate—for our calculation is carried out in the context of SQED—, we have assigned the neutralino mass to the photino. In any case, the electron mass could be neglected compared with the sparticle masses, and (37) simplifies to

$$\frac{\mathrm{d}\sigma}{\mathrm{d}\Omega}(e^-e^+ \to \tilde{\gamma}\tilde{\gamma}) = \frac{\alpha^2}{4s}\sqrt{1-\left(\frac{2m_{\tilde{\gamma}}}{\sqrt{s}}\right)^2}\left[\left(\frac{t-m_{\tilde{\gamma}}^2}{t-M_{\tilde{e}}^2}\right)^2 + \left(\frac{u-m_{\tilde{\gamma}}}{u-M_{\tilde{e}}^2}\right)^2 - \frac{2sm_{\tilde{\gamma}}^2}{(u-M_{\tilde{e}}^2)(t-M_{\tilde{e}}^2)}\right], \quad (38)$$

which is the result in [34, 35]. In addition, with $m_{\tilde{\gamma}} = 0$, we obtain (4), the result derived by Fayet [33].

The total cross section for the process $e^-e^+ \to \tilde{\gamma}\tilde{\gamma}$ is given by [35]

$$\sigma(e^-e^+ \to \tilde{\gamma}\tilde{\gamma}) = \frac{2\pi\alpha^2}{s^2}\left\{\mathcal{S} + 2\Delta\Lambda + \frac{\mathcal{S}\Delta^2}{m_{\tilde{\gamma}}^4 + M_{\tilde{e}}^4 + M_{\tilde{e}}^2(s-2m_{\tilde{\gamma}}^2)} + 2\frac{m_{\tilde{\gamma}}^2 s\Lambda)}{s+2\Delta}\right\}, \quad (39)$$

where

$$\mathcal{S} = \sqrt{s(s-4m_{\tilde{\gamma}}^2)},$$
$$\Delta = M_{\tilde{e}}^2 - m_{\tilde{\gamma}}^2,$$
$$\Lambda = \ln\left[\frac{s+2\Delta-\mathcal{S}}{s+2\Delta+\mathcal{S}}\right]. \quad (40)$$

The so-called international linear collider (ILC) will provide opportunities for both discovery and precision measurements [62]. With the construction of the next generation of e^+e^- linear colliders, with a center-of-mass energy up to 1.5 TeV, capable of operating also in the $\gamma\gamma$, γe^-, and e^-e^- modes, new perspectives arise for detecting new physics beyond the standard model in processes having nonzero initial electric charge (and nonzero lepton number).

If the photino is stable, then all supersymmetric cascade processes ultimately decay into photinos. The photino is unseen as it leaves the detector, and its existence can only be inferred by looking for unbalanced momentum in a detector. In this way, it is phenomenologically similar to neutrinos. The events produced by the photinos display large discrepancy in energy and momentum between the visible initial- and final-state particles. Nowadays, this is the signature of the LSP, which, depending on the scenario, can be the lightest neutralino ($\tilde{\chi}_1^0$), the gravitino (the supersymmetric partner of the graviton), or the lightest sneutrino $\tilde{\nu}_1$, i.e., the supersymmetric partners of neutrinos. On the other hand, in certain minimal supergravity (mSUGRA) scenarios, the LSP can be a light photino (this means that $\tilde{\chi}_1^0 \approx \tilde{\gamma}$) [50–52] with an acceptable cosmological abundance [61].

In the following, we shall present our numerical results assuming the photino to be the lightest neutralino of the MSSM. In the SPS scenarios, its mass ranges between 70 and 200 GeV, whereas the selectron mass ranges from 200 GeV to 1.5 TeV (see Table 1).

In Fig. 6, we show results for the total cross section of photino production as a function of the photino and selectron masses, for three different CM energies. To study the dependence on the photino mass, we fix $M_{\tilde{e}} =$ 202 GeV for the selectron mass (SPS1a scenario). The cross sections for $\sqrt{s} = 0.5$ TeV are largest, the results for $\sqrt{s} = 1$ and $\sqrt{s} = 1.5$ TeV being insensitive to the photino mass. For the dependency on the selectron mass, we use $M_{\tilde{\gamma}} = 96$ GeV for the photino mass. For $M_{\tilde{e}} > 800$ GeV, the cross sections for $\sqrt{s} = 1$ and $\sqrt{s} =$ 1.5 TeV are very close to each other, but the results differ for lighter selectron masses. For $\sqrt{s} = 0.5$ TeV, the cross section grows up faster than in the previous cases for decreasing selectron masses. In conclusion, if the selectron mass is not much heavier than $M_{\tilde{e}} \simeq$ 500 GeV, the ILC with $\sqrt{s} = 0.5$ TeV is likely to discover the lightest neutralinos and to place constraints on the selectron mass.

Let us now estimate the number of photinos that will be produced in the future ILC. Given the expected luminosity of $\mathcal{L} = 1.5 \times 10^{34}$ cm^{-2}s^{-1} [63] for the 0.5-TeV mode, in 1 year (10^7 s) 65,218 photinos will be produced in the more optimistic SPS1 scenario and 525 photinos in the less optimistic SPS2 scenario.

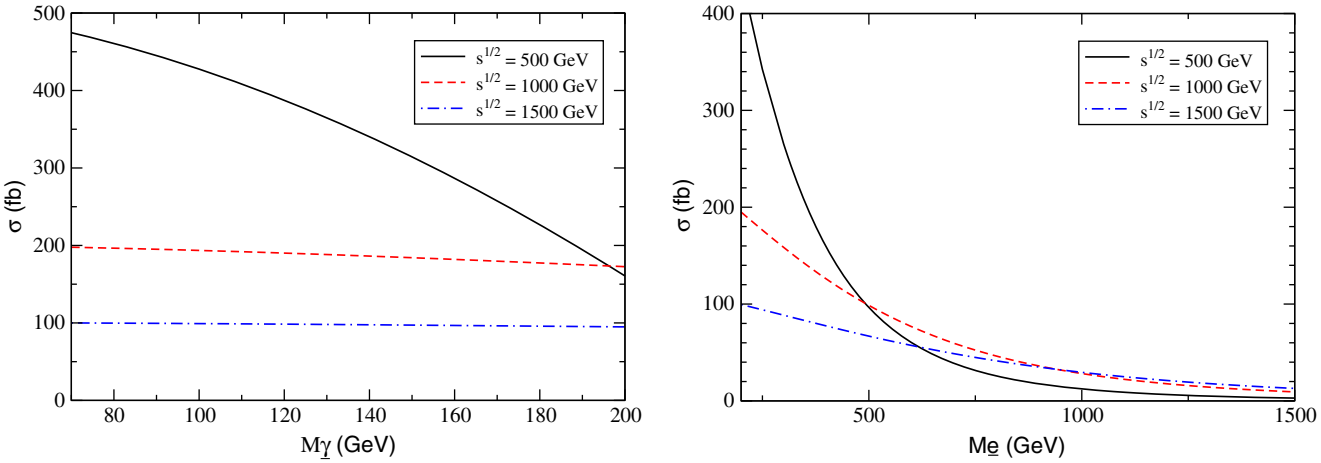

Fig. 6 Total cross section of photino production in e^-e^+ collisions for different CM energies: $\sqrt{s} = 0.5$ TeV (*solid line*), for $\sqrt{s} = 1.0$ TeV (*dashed line*), and for $\sqrt{s} = 1.5$ TeV (*dot-dashed line*). *Left panel*: Cross section as a function of the photino mass, for $M_{\tilde{e}} = 400$ GeV. *Right panel*: Cross section as a function of the selectron mass, for $M_{\tilde{\gamma}} = 79$ GeV

4 Gluino Production in the MSSM

Gluino and squark production in hadron colliders dominantly occurs via strong interactions. Thus, their production rate may be expected to be considerably larger than for sparticles with electroweak interactions only, whose production has been studied in the literature.

The cross sections for the production of gluinos and squarks in hadron collisions were calculated at the Born level quite some time ago [35] and in the next-to-leading order (NLO) accuracy more recently [64] . In the present study, as another example of detailed calculation, we consider the inclusive production of gluinos in *pp* collisions. For more detailed descriptions of the procedures, see [65, 66].

We do not consider in detail the top squark production, for which our assumptions are invalid, so that more involved treatment is required [67]. In the following, we detail the steps necessary to calculate the various contributing subprocesses.

4.1 Subprocess $\bar{q}q \to \tilde{g}\tilde{g}$

The Feynman diagrams for gluino pair production coming from quark–antiquark initial states are drawn in Fig. 7. We denote the initial-state quark and antiquark momenta, spin and color by (k_1, s_1, a) and (k_2, s_2, b), and the final-state gluino momenta and spin by (P_1, s_3, e) and (P_2, s_4, d), respectively.

The Mandelstam variables are

$$
\begin{aligned}
s &= (k_1 + k_2)^2 = (P_1 + P_2)^2 = 2k_1 \cdot k_2 = 2m_{\tilde{g}}^2 \\
&\quad + 2P_1 \cdot P_2 = 4E^2, \\
t &= (k_1 - P_1)^2 = (P_2 - k_2)^2 = m_{\tilde{g}}^2 - 2k_1 \cdot P_1 = m_{\tilde{g}}^2 - 2k_2 \cdot P_2 \\
&= m_{\tilde{g}}^2 - 2E^2 + 2E\sqrt{E^2 - m_{\tilde{g}}^2}\cos\theta, \\
u &= (k_1 - P_2)^2 = (P_1 - k_2)^2 = m_{\tilde{g}}^2 - 2k_1 \cdot P_2 = m_{\tilde{g}}^2 - 2k_2 \cdot P_1 \\
&= m_{\tilde{g}}^2 - 2E^2 - 2E\sqrt{E^2 - m_{\tilde{g}}^2}\cos\theta, \\
s + t + u &= 2m_{\tilde{g}}^2,
\end{aligned}
\tag{41}
$$

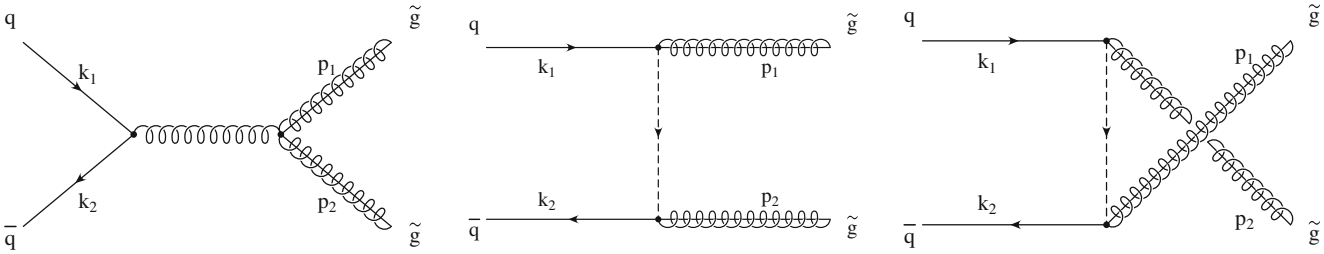

Fig. 7 Feynman diagrams for gluino pair production quark–antiquark initial states

where E is the center-of-mass energy of the colliding quarks, $m_{\tilde{g}}$ is the gluino mass, and θ is the scattering angle.

The expressions for the amplitudes in these subprocesses are

$$\begin{aligned}
\mathcal{M}_s &= (-\imath g_s)\left(w^\dagger(b)\bar{v}(k_2,s_2)T^c\gamma_m w(a)u(k_1,s_1)\right)\\
&\quad\cdot\left(\frac{g^{mn}\delta^{cg}}{s}\right)(-\imath g_s)\\
&\quad\cdot\left(\Omega_g^\dagger(d)\bar{u}(P_2,s_4)\,f^{deg}\gamma_n\Omega_g(e)u(P_1,s_3)\right)\\
&= -\frac{g_s^2}{s}\left(\bar{v}(k_2,s_2)\gamma_m u(k_1,s_1)\right)\left(\bar{u}(P_2,s_4)\gamma^m u(P_1,s_3)\right)\\
&\quad\cdot\left(w^\dagger(b)T^c w(a)\right)\left(f^{dec}\Omega_g^\dagger(d)\Omega_g(e)\right),\\
\mathcal{M}_t &= \left(-\imath\sqrt{2}g_s(L-R)\right)\left(w^\dagger(b)\bar{v}(k_2,s_2)T^c\Omega_c(d)u(P_2,s_4)\right)\\
&\quad\cdot\left(\frac{\imath\delta^{cf}}{t-M_{\tilde{q}}^2}\right)(-\imath\sqrt{2}g_s(L-R))\\
&\quad\cdot\left(\Omega_f^\dagger(e)\bar{u}(P_1,s_3)T^f w(a)u(k_1,s_1)\right)\\
&= -\frac{2\imath g_s^2}{t-M_{\tilde{q}}^2}\left(\bar{v}(k_2,s_2)(L-R)u(P_2,s_4)\right)\left(\bar{u}(P_1,s_4)\right.\\
&\quad\left.\cdot(L-R)u(k_1,s_1)\right)\left(w^\dagger(b)T^c\Omega_c(d)\right)\left(\Omega_c^\dagger(e)T^c w(a)\right)\\
&= -\frac{2\imath g_s^2}{t-M_{\tilde{q}}^2}(L+R)^2\left(\bar{v}(k_2,s_2)u(P_2,s_4)\right)\\
&\quad\cdot\left(\bar{u}(P_1,s_4)u(k_1,s_1)\right)\left(w^\dagger(b)T^c\Omega_c(d)\right)\left(\Omega_c^\dagger(e)T^c w(a)\right)\\
&= -\frac{4\imath g_s^2}{t-M_{\tilde{q}}^2}\left(\bar{v}(k_2,s_2)u(P_2,s_4)\right)\left(\bar{u}(P_1,s_4)u(k_1,s_1)\right)\\
&\quad\cdot\left(w^\dagger(b)T^c\Omega_c(d)\right)\left(\Omega_c^\dagger(e)T^c w(a)\right),\\
\mathcal{M}_u &= -(-\imath\sqrt{2}g_s(L-R))(-\imath\sqrt{2}g_s(L-R))\\
&\quad\cdot\left(w^\dagger(b)\bar{v}(k_2,s_2)T^c\Omega_c(e)u(P_1,s_3)\right)\\
&\quad\cdot\left(\frac{\imath\delta^{cf}}{u-M_{\tilde{q}}^2}\right)\left(\Omega_f^\dagger(d)\bar{u}(P_2,s_4)T^f w(a)u(k_1,s_1)\right)\\
&= +\frac{4\imath g_s^2}{t-M_{\tilde{q}}^2}\left(\bar{v}(k_2,s_2)u(P_1,s_3)\right)\left(\bar{u}(P_2,s_4)u(k_1,s_1)\right)\\
&\quad\cdot\left(w^\dagger(b)T^c\Omega_c(e)\right)\left(\Omega_c^\dagger(d)T^c w(a)\right),
\end{aligned}\tag{42}$$

where $w(a)$ and $\Omega(a)$ are the color wavefunctions of the quarks and gluinos, respectively [15].

The $\Omega(a)$'s are 8×8 matrices, in the octet representations of the $SU(3)_C$ group, satisfying the following relations

$$\begin{aligned}
(\Omega(a))_{bc} &= -\imath f_{abc},\\
\left[\Omega(a),\Omega(b)\right] &= \imath f_{abc}\Omega(c).
\end{aligned}\tag{43}$$

The total amplitude is given by

$$\mathcal{M} = \mathcal{M}_s + \mathcal{M}_t + \mathcal{M}_u.\tag{44}$$

Defining the appropriate color factors

$$\begin{aligned}
G_s &\equiv \frac{g_s^2}{s}\left(w^\dagger(b)T^g w(a)\right)\left(f^{deg}\Omega_g^\dagger(d)\Omega_g(e)\right),\\
G_t &\equiv \frac{g_s^2}{t-M_{\tilde{q}}^2}\left(w^\dagger(b)T^c\Omega_c(d)\right)\left(\Omega_c^\dagger(e)T^c w(a)\right),\\
G_u &\equiv \frac{g_s^2}{u-M_{\tilde{q}}^2}\left(w^\dagger(b)T^c\Omega_c(e)\right)\left(\Omega_c^\dagger(d)T^c w(a)\right),
\end{aligned}\tag{45}$$

and the following flavor factors

$$\begin{aligned}
S_s &= \left(\bar{v}(k_2,s_2)\gamma_m u(k_1,s_1)\right)\left(\bar{u}(P_2,s_4)\gamma^m u(P_1,s_3)\right),\\
S_t &= \left(\bar{v}(k_2,s_2)u(P_2,s_4)\right)\left(\bar{u}(P_1,s_3)u(k_1,s_1)\right),\\
S_u &= \left(\bar{v}(k_2,s_2)u(P_1,s_3)\right)\left(\bar{u}(P_2,s_4)u(k_1,s_1)\right),
\end{aligned}$$

we can rewrite the amplitude (44) in the form

$$\mathcal{M} = S_s G_s + 4\imath S_t G_t - 4\imath S_u G_u\,.\tag{46}$$

Squaring this amplitude and summing over initial and final color and spins, we are led to the expression

$$\begin{aligned}
\sum_{s_1,s_2,s_3,s_4}|\mathcal{M}|^2 &= |S_s|^2|G_s|^2 + 4\imath S_s^* S_t G_s^* G_t - 16\imath S_s^* S_u G_s^* G_u\\
&\quad - 4\imath S_s S_t^* G_s G_t^* + 16|S_t|^2|G_t|^2\\
&\quad - 16 S_t^* S_u G_t^* G_u\\
&\quad + 4\imath S_s S_u^* G_s G_u^* + 16|S_u|^2|G_u|^2.
\end{aligned}\tag{47}$$

Let us first examine the flavor factors. The usual quantum field-theory techniques yield the equalities

$$\begin{aligned}
\sum_{s_1,s_2,s_3,s_4} |S_s|^2 &= \mathrm{Tr}\left[\not{k}_2\gamma_m\ \not{k}_1\gamma_n\right] \\
&\quad\times \mathrm{Tr}\left[(\not{P}_2+m_{\tilde{g}})\gamma^m(\not{P}_1+m_{\tilde{g}})\gamma^n\right] \\
&= k_2^o k_2^p \mathrm{Tr}\left[\gamma_o\gamma_m\gamma_p\gamma_n\right] \\
&\quad+\mathrm{Tr}\Big[\not{P}_2\gamma^m\ \not{P}_1\gamma^n + m_{\tilde{g}}^2\gamma^m\gamma^n \\
&\qquad+ m_{\tilde{g}}\left(\not{P}_2\gamma^m\gamma^n+\gamma^m\ \not{P}_1\gamma^n\right)\Big] \\
&= \left[4\cdot(k_{2m}k_{1n}-g_{mn}k_1\cdot k_2+k_{2n}k_{1m})\right] \\
&\quad\cdot\left[4\cdot\left(P_2^mP_1^n-g^{mn}P_1\cdot P_2+P_2^nP_1^m+m_{\tilde{g}}^2g^{mn}\right)\right] \\
&= 32\left[(k_1\cdot P_1)(k_2\cdot P_2)+(k_1\cdot P_2)(k_2\cdot P_1)\right. \\
&\qquad\left.+\ m_{\tilde{g}}^2\left(k_1\cdot k_2+2m_{\tilde{g}}^2\right)\right] \\
&= 8\left[\left(m_{\tilde{g}}^2-t\right)^2+\left(m_{\tilde{g}}^2-u\right)^2+2sm_{\tilde{g}}^2\right],
\end{aligned}$$

$$\begin{aligned}
\sum_{s_1,s_2,s_3,s_4} S_s^*S_t = S_t^*S_s &= \mathrm{Tr}\left[\not{k}_2\gamma_m\not{k}_1(\not{P}_1+m_{\tilde{g}})\gamma^m(\not{P}_2+m_{\tilde{g}})\right] \\
&= \mathrm{Tr}\Big[\not{k}_2\gamma_m\ \not{k}_1\ \not{P}_1\gamma^m\ \not{P}_2+m_{\tilde{g}}\not{k}_2\gamma_m\ \not{k}_1\ \not{P}_1\gamma^m \\
&\qquad+m_{\tilde{g}}\ \not{k}_2\gamma_m\ \not{k}_1\gamma^m\ \not{P}_2+m_{\tilde{g}}^2\ \not{k}_2\gamma_m\ \not{k}_1\gamma^m\Big] \\
&= 16\,(k_1\cdot P_1)\,(k_2\cdot P_2)+m_{\tilde{g}}^2\,(k_1\cdot k_2) \\
&= 4\left(m_{\tilde{g}}^2-t\right)+m_{\tilde{g}}^2 s,
\end{aligned}$$

$$\begin{aligned}
\sum_{s_1,s_2,s_3,s_4} S_s^*S_u = S_u^*S_s &= \mathrm{Tr}\left[\not{k}_2\gamma_m\ \not{k}_1(\not{P}_2+m_{\tilde{g}})\gamma^m(\not{P}_1+m_{\tilde{g}})\right] \\
&= \mathrm{Tr}\Big[\ \not{k}_2\gamma_m\ \not{k}_1\ \not{P}_2\gamma^m\ \not{P}_1+m_{\tilde{g}}\ \not{k}_2\gamma_m\ \not{k}_1\ \not{P}_2\gamma^m \\
&\quad+\ m_{\tilde{g}}\ \not{k}_2\gamma_m\ \not{k}_1\gamma^m\ \not{P}_1+m_{\tilde{g}}^2\ \not{k}_2\gamma_m\ \not{k}_1\gamma^m\Big] \\
&= 16\,(k_1\cdot P_2)\,(k_2\cdot P_1)+m_{\tilde{g}}^2\,(k_1\cdot k_2) \\
&= 4\left(m_{\tilde{g}}^2-u\right)+m_{\tilde{g}}^2 s,
\end{aligned}$$

$$\begin{aligned}
\sum_{s_1,s_2,s_3,s_4} |S_t|^2 &= \mathrm{Tr}\left[\not{k}_2(\not{P}_2+m_{\tilde{g}})\right]\ \mathrm{Tr}\left[(\not{P}_1+m_{\tilde{g}})\ \not{k}_1\right] \\
&= \mathrm{Tr}\left[\not{k}_1\ \not{P}_1\right]+\mathrm{Tr}\left[\not{k}_2\ \not{P}_2\right] \\
&\quad+m_{\tilde{g}}\left\{\mathrm{Tr}\left[\not{k}_1\right]+\mathrm{Tr}\left[\not{k}_2\right]\right\} \\
&= 4\left[P_1\cdot k_1+P_2\cdot k_2\right] \\
&= 4\left(m_{\tilde{g}}^2-t\right),
\end{aligned}$$

$$\begin{aligned}
\sum_{s_1,s_2,s_3,s_4} S_s^*S_u = S_u^*S_s &= \mathrm{Tr}\left[\not{k}_1\ \not{P}_1\right]\mathrm{Tr}\left[\not{k}_2\ \not{P}_1\right] \\
&\quad-\mathrm{Tr}\left[\not{k}_1\ \not{P}_2\right]\mathrm{Tr}\left[\not{k}_2\ \not{P}_2\right]+m_{\tilde{g}}^2\mathrm{Tr}\left[\not{k}_1\ \not{k}_2\right] \\
&= 4\Big[\ (k_1\cdot P_1)\,(k_2\cdot P_1)-(k_1\cdot P_2)\,(k_2\cdot P_2) \\
&\qquad+\ m_{\tilde{g}}^2\,(k_1\cdot k_2)\Big] \\
&= 8sm_{\tilde{g}}^2,
\end{aligned}$$

$$\begin{aligned}
\sum_{s_1,s_2,s_3,s_4} |S_u|^2 &= \mathrm{Tr}\left[(\not{P}_2+m_{\tilde{g}})\ \not{k}_1\right]\ \mathrm{Tr}\left[(\not{P}_1+m_{\tilde{g}})\ \not{k}_2\right] \\
&= \mathrm{Tr}\left[\not{k}_1\ \not{P}_2\right]+\mathrm{Tr}\left[\not{k}_2\ \not{P}_1\right] \\
&\quad+m_{\tilde{g}}\left\{\mathrm{Tr}\left[\not{k}_1\right]+\mathrm{Tr}\left[\not{k}_2\right]\right\} \\
&= 4\left[P_2\cdot k_1+P_1\cdot k_2\right] \\
&= 4\left(m_{\tilde{g}}^2-u\right). \qquad (48)
\end{aligned}$$

Consider next the color factors. Apart from the averaging factor (1/9), we get the following results:

$$\begin{aligned}
\sum_{a,b,d,e} |G_s|^2 &= \frac{g_s^4}{4s^2}\mathrm{Tr}\left[\lambda^c\lambda^g\right] f^{dec}\,f^{dec'}\,f^{deg}\,f^{deg'} \\
&= \frac{g_s^4}{4s^2}\cdot 16\cdot 72, \\
\sum_{a,b,d,e} G_s^*G_t &= \sum_{a,b,d,e} G_sG_t^* = \frac{g_s^4}{s\left(t-M_{\tilde{q}}^2\right)}\cdot 16\cdot 72, \\
\sum_{a,b,d,e} G_s^*G_u &= \sum_{a,b,d,e} G_sG_u^* = \frac{g_s^4}{s\left(u-M_{\tilde{q}}^2\right)}\cdot 16\cdot 72, \\
\sum_{a,b,d,e} |G_t|^2 &= \frac{g_s^4}{\left(t-M_{\tilde{q}}^2\right)^2}\cdot 16\cdot 72\cdot\frac{3}{9}, \\
\sum_{a,b,d,e} G_t^*G_u &= \sum_{a,b,d,e} G_tG_u^* = \frac{g_s^4}{\left(t-M_{\tilde{q}}^2\right)\left(u-M_{\tilde{q}}^2\right)}\cdot 16\cdot 72, \\
\sum_{a,b,d,e} |G_u|^2 &= \frac{g_s^4}{4\left(u-M_{\tilde{q}}^2\right)^2}\cdot 16\cdot 72\cdot\frac{3}{9}. \qquad (49)
\end{aligned}$$

We may now substitute (48), (49), and (46) into the usual expression for the differential cross section,

$$\frac{\mathrm{d}\sigma}{\mathrm{d}t} = \frac{1}{16\pi s^2}\left(\frac{1}{64}\sum_{a,b,d,e}\frac{1}{4}\sum_{s_1,s_2,s_3,s_4}|\mathcal{M}|^2\right). \qquad (50)$$

We have checked that our analytical calculations agree with the results of the FeynArts program [58], with the MSSM code [68]. Finally, we find the following expression:

$$\begin{aligned}\frac{\mathrm{d}\sigma}{\mathrm{d}\hat{t}}(\bar{q}q\to\tilde{g}\tilde{g}) &= \frac{8\pi\alpha_s^2}{9\hat{s}^2}\left\{\frac{4}{3}\left(\frac{m_{\tilde{g}}^2-\hat{t}}{M_{\tilde{q}}^2-\hat{t}}\right)^2+\frac{4}{3}\left(\frac{m_{\tilde{g}}^2-\hat{u}}{M_{\tilde{q}}^2-\hat{u}}\right)^2\right.\\ &\quad+\frac{3}{\hat{s}^2}\left[(m_{\tilde{g}}^2-\hat{t})^2+(m_{\tilde{g}}^2-\hat{u})^2+2m_{\tilde{g}}^2\hat{s}\right]\\ &\quad-3\left[\frac{(m_{\tilde{g}}^2-\hat{t})^2+m_{\tilde{g}}^2\hat{s}}{\hat{s}(M_{\tilde{q}}^2-\hat{t})}\right]\\ &\quad-3\left[\frac{(m_{\tilde{g}}^2-\hat{u})^2+m_{\tilde{g}}^2\hat{s}}{\hat{s}(M_{\tilde{q}}^2-\hat{u})}\right]\\ &\quad\left.+\frac{1}{3}\frac{m_{\tilde{g}}^2\hat{s}}{(M_{\tilde{q}}^2-\hat{t})(M_{\tilde{q}}^2-\hat{u})}\right\}. \end{aligned}\tag{51}$$

These results agree with those in Refs. [14, 35].

4.2 Subprocess $gg\to\tilde{g}\tilde{g}$

The Feynman diagrams for gluino production coming from gluon fusion are depicted in Fig. 8. The initial-state gluons have $SU(3)_C$ adjoint representation indices a and b, with momenta k_1 and k_2 and polarization vectors $\varepsilon_1^m(k_1,\lambda_1)$ and $\varepsilon_2^m(k_2,\lambda_2)$, respectively. The final-state gluinos carry adjoint representation indices c and d, with momenta P_3 and P_4.

The Feynman amplitudes are given by

$$\begin{aligned}\mathcal{M}_s &= (-\imath g_s f^{abe})\left(\epsilon_m(k_1)w^a(c)\epsilon_n^*(k_2)w^b(c)\right)\left(\frac{g^{mn}\delta^{ef}}{s}\right)\\ &\quad\times(-\imath g_s f^{cdf})\left(\Omega^\dagger(c)\bar{u}(P_1)\Omega(d)u(P_2)\right)\\ &\quad\cdot\left[g_{mn}(P_1-P_2)_r+g_{nr}(P_2+Q)_m-g_{rm}(Q+P_1)_r\right],\\ \mathcal{M}_t &= (-\imath g_s f^{bde})\left(\epsilon_m(k_2)w^b(c)u(P_2)\Omega(d)\right)\\ &\quad\times\left(\frac{\imath(\not{q}+m_{\tilde{g}})}{t-m_{\tilde{g}}^2}\delta^{de}g^{mn}\right)(-\imath g_s f^{bcf})\\ &\quad\cdot\left(\bar{u}(k_1)\Omega^\dagger(c)\epsilon_n(k_1)w^a(c)\right),\\ \mathcal{M}_u &= (-\imath g_s f^{bce})\left(\epsilon_m(k_2)w^b(c)u(k_1)\Omega(c)\right)\\ &\quad\times\left(\frac{\imath(\not{q}+m_{\tilde{g}})}{u-m_{\tilde{g}}^2}\delta^{de}g^{mn}\right)(-\imath g_s f^{bdf})\\ &\quad\cdot\left(\bar{u}(k_2)\Omega^\dagger(d)\epsilon_n(k_1)w^a(c)\right). \end{aligned}\tag{52}$$

Before presenting our results for this case, we find it interesting to present a brief review of the polarization vectors used to describe real photons as well as real gluons. We choose to work with real transverse polarization vectors ε_1 and ε_2, both of which must be orthogonal to the initial-state collision axis in the center-of-momentum frame. We can, hence, write the following relations:

$$\begin{aligned}&\varepsilon_i\cdot\varepsilon_j=-\delta_{ij},\\ &\varepsilon_1\cdot p_1=\varepsilon_2\cdot p_1=\varepsilon_1\cdot p_2\\ &\qquad=\varepsilon_2\cdot p_2=0\ \ \text{(Lorentz condition)},\\ &\varepsilon_1\cdot k_2=-\varepsilon_1\cdot k_1,\\ &\varepsilon_2\cdot k_2=-\varepsilon_2\cdot k_1, \end{aligned}\tag{53}$$

for each choice of λ_1 and λ_2.

Summing over gluon polarizations, one has that

$$\begin{aligned}&\sum_{\lambda_1,\lambda_2}1=4,\qquad\qquad\sum_{\lambda_1,\lambda_2}(\varepsilon_1\cdot\varepsilon_2)^2=2,\\ &\sum_{\lambda_1,\lambda_2}(\varepsilon_1\cdot\varepsilon_2)(k_1\cdot\varepsilon_1)(k_1\cdot\varepsilon_2)=m_{\tilde{g}}^2-\frac{(t-m_{\tilde{g}}^2)(u-m_{\tilde{g}}^2)}{s}, \end{aligned}\tag{54}$$

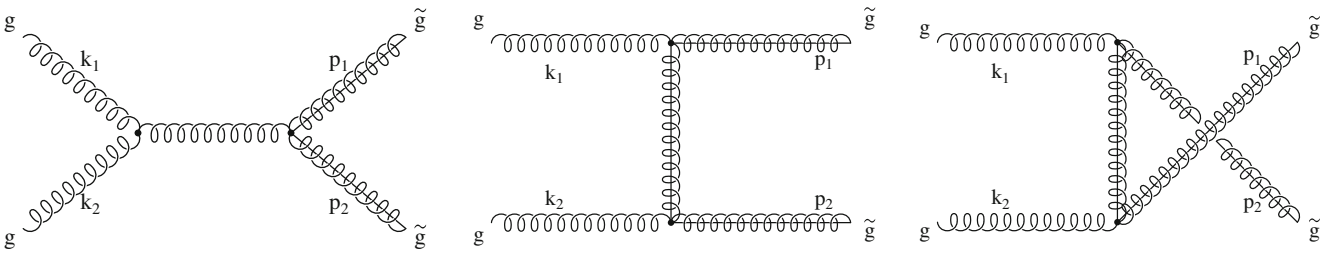

Fig. 8 Feynman diagrams for gluino pair production gluon–gluon initial states

$$\sum_{\lambda_1,\lambda_2}(k_1\cdot\varepsilon_1)^2(k_1\cdot\varepsilon_2)^2=\left(m_{\tilde{g}}^2-\frac{(t-m_{\tilde{g}}^2)(u-m_{\tilde{g}}^2)}{s}\right)^2. \quad (55)$$

Following the procedure adopted in the Section 4.1 and taking advantage of the following expressions [28],

$$\sum_{\text{colors}} G_s^2=\frac{72g_s^4}{s^2}, \qquad \sum_{\text{colors}} G_t^2=\frac{72g_s^4}{(t-m_{\tilde{g}}^2)^2}, \quad (56)$$

$$\sum_{\text{colors}} G_u^2=\frac{72g_s^4}{(u-m_{\tilde{g}}^2)^2}, \qquad \sum_{\text{colors}} G_sG_t=\frac{36g_s^4}{s(t-m_{\tilde{g}}^2)}, \quad (57)$$

$$\sum_{\text{colors}} G_sG_u=-\frac{36g_s^4}{s(u-m_{\tilde{g}}^2)},$$

$$\sum_{\text{colors}} G_tG_u=\frac{36g_s^4}{(t-m_{\tilde{g}}^2)(u-m_{\tilde{g}}^2)}, \quad (58)$$

we come to the following differential cross section for the case under study, which we have also checked with FeynCalc:

$$\begin{aligned}\frac{\mathrm{d}\sigma}{\mathrm{d}\hat{t}}(gg\to\tilde{g}\tilde{g}) &= \frac{9\pi\alpha_s^2}{4\hat{s}^2}\left\{\frac{2(m_{\tilde{g}}^2-\hat{t})(m_{\tilde{g}}^2-\hat{u})}{\hat{s}^2}+\frac{m_{\tilde{g}}^2(\hat{s}-4m_{\tilde{g}}^2)}{(m_{\tilde{g}}^2-\hat{t})(m_{\tilde{g}}^2-\hat{u})}\right.\\ &+\frac{(m_{\tilde{g}}^2-\hat{t})(m_{\tilde{g}}^2-\hat{u})+2m_{\tilde{g}}^2(m_{\tilde{g}}^2+\hat{t})}{(m_{\tilde{g}}^2-\hat{t})^2}\\ &+\frac{(m_{\tilde{g}}^2-\hat{t})(m_{\tilde{g}}^2-\hat{u})+2m_{\tilde{g}}^2(m_{\tilde{g}}^2+\hat{u})}{(m_{\tilde{g}}^2-\hat{u})^2}\\ &+\frac{(m_{\tilde{g}}^2-\hat{t})(m_{\tilde{g}}^2-\hat{u})+m_{\tilde{g}}^2(\hat{u}-\hat{t})}{\hat{s}(m_{\tilde{g}}^2-\hat{t})}\\ &\left.+\frac{(m_{\tilde{g}}^2-\hat{t})(m_{\tilde{g}}^2-\hat{u})+m_{\tilde{g}}^2(\hat{u}-\hat{t})}{\hat{s}(m_{\tilde{g}}^2-\hat{u})}\right\}. \quad (59)\end{aligned}$$

Once again, the result agrees with the expressions in Refs. [14, 35].

4.3 Subprocess $qg\to\tilde{q}\tilde{g}$

The Feynman diagrams for gluino production from Compton scattering qg are shown in Fig. 9.

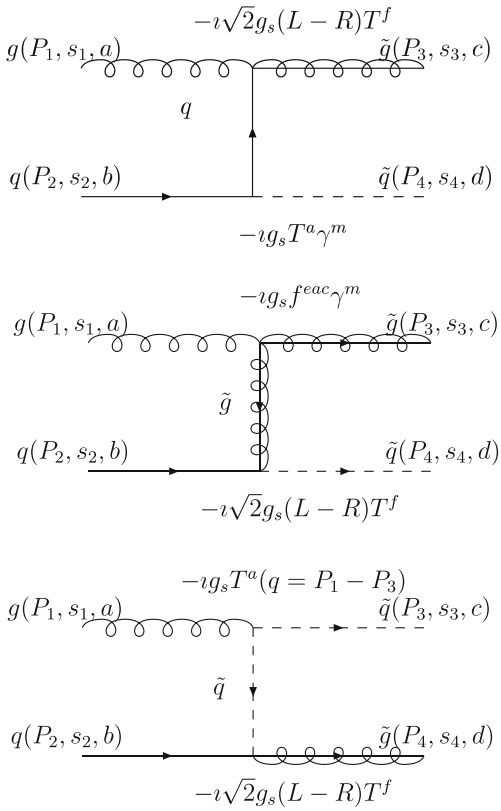

Fig. 9 Feynman diagrams for squark–gluino production. The *arrows* indicate the fermion flow

The Feynman amplitudes are given by the equalities

$$\begin{aligned}\mathcal{M}_s &= (-\imath\sqrt{2}g_s(L-R))\left(w^\dagger(d)T^fw(c)u(P_3,s_3)\right)\\ &\times\left(\frac{\imath(\not{q}+m_{\tilde{g}})}{s}\delta^{fe}\right)(-\imath g_sf^{eac})\\ &\cdot\left(\Omega^\dagger(a)\bar{u}(P_1,s_1))T^e\gamma^m\epsilon^n(P_2)w^e(b)\right),\\ \mathcal{M}_t &= (-\imath\sqrt{2}g_s(L-R))\left(w^\dagger(d)T^fw(b)u(P_2,s_2)\right)\\ &\times\left(\frac{\imath(\not{q}+m_{\tilde{g}})}{t-m_{\tilde{g}}^2}\delta^{fe}\right)(-\imath g_sf^{eac})\\ &\cdot\left(\epsilon^{mu}(P_1)w^e(a)\gamma^{mu}u(P_3,s_3))\Omega(c)\right),\\ \mathcal{M}_u &= (-\imath\sqrt{2}g_s(L-R))\left(w^\dagger(d)T^fw(b)u(P_3,s_3)\right)\\ &\times\left(\frac{\imath(\not{q}+m_{\tilde{g}})}{u-m_{\tilde{g}}^2}\delta^{fe}\right)(-\imath g_sf^{eac})\\ &\cdot\left(\epsilon^{mu}(P_1)w^e(a)\gamma^{mu}u(P_4,s_4))\Omega(c)\right). \quad (60)\end{aligned}$$

The differential cross section for the Compton-like subprocesses is then given by

$$\frac{\mathrm{d}\sigma}{\mathrm{d}\hat{t}}(qg \to \tilde{q}\tilde{g}) = \frac{\pi\alpha_s^2}{24\hat{s}^2}\left\{\left[\frac{\frac{16}{3}(\hat{s}^2+(m_{\tilde{q}}^2-\hat{u})^2)+\frac{4}{3}\hat{s}(M_{\tilde{q}}^2-\hat{u})}{\hat{s}(m_{\tilde{g}}^2-\hat{t})(m_{\tilde{g}}^2-\hat{u})}\right]\times\left((m_{\tilde{g}}^2-\hat{u})^2+(M_{\tilde{q}}^2-m_{\tilde{g}}^2)^2+\frac{2\hat{s}m_{\tilde{g}}^2(M_{\tilde{q}}^2-m_{\tilde{g}}^2)}{(m_{\tilde{g}}^2-\hat{t})}\right)\right\}, \quad (61)$$

in agreement with Refs. [14, 35].

The total cross section for gluino production can be obtained by adding (51), (59), and (61) and integrating the resulting equality over phase space, which yields the results in Refs. [35, 64]. We have used these expressions to find the results presented in Refs. [65, 66, 69].

The central purpose of the LHC [70], which is already running and soon will be fully operative with 14-TeV energy, is to find the Higgs particle. That discovery may either confirm the SM or open new windows towards new physics. This machine will also study collisions involving nuclei-pA (proton–nucleus, $\sqrt{s} = 8.8$ TeV) and AA (nucleus–nucleus, $\sqrt{s} = 5.5$ TeV) LHC modes. Results for gluino production in the pA and AA modes were presented for the first time in Refs. [66, 69].

Before presenting our numerical results on gluino production at the LHC, we recall that gluon fluxes and large color factors make gluon–gluon (gg) fusion contributions dominant at LHC energies if $m_{\tilde{g}}$, $M_{\tilde{q}} \leq 1$ TeV, while reactions involving valence quarks dominate gluino production at the Tevatron in the allowed mass range. The rate of gluino pair production is maximized for $m_{\tilde{g}} \simeq M_{\tilde{q}}$ [11].

Figure 10 shows the LO QCD total cross section for gluino production at the LHC as a function of the gluino masses. The continuous curves display the cross sections calculated for the CTEQ6L parton densities [71], with the indicated assumptions on the squark masses and choices of the hard scale. For $m_{\tilde{q}} = m_{\tilde{g}}$, the solid, dotted, and dash-dotted curves monitor the sensitivity to the hard scale. Our curves are qualitatively equivalent to the ones in chapter 12 of Ref. [14], based on the CTEQ5L parton distribution.

Since the pp CM energy $\sqrt{s} = 14$ TeV is several times larger than the expected gluino and squark masses, these particles may well be produced and detected at the LHC. The expected luminosity for the full LHC performance is $\mathcal{L} \approx 10^{34}$ cm^{-2} s^{-1}, which is

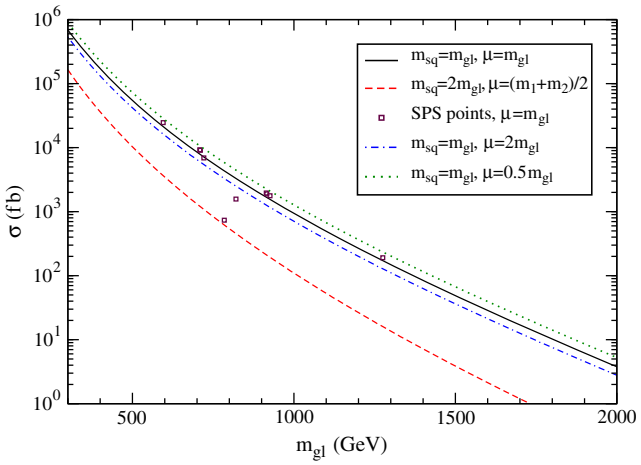

Fig. 10 Total LO cross section for gluino production at the LHC as a function of the gluino masses. Parton densities: CTEQ6L, with two assumptions on the squark masses and choices of the hard scale (*curves*). For $m_{\tilde{q}} = m_{\tilde{g}}$, the sensitivity to the hard scale is also presented . The *open squares* show the numerical results for the SPS points (see Table 1)

equivalent to 100 fb^{-1}, assuming a full LHC year of 10^7 s. Considering the SPS1a scenario (lightest gluino of mass 595.2 GeV), roughly $2 \cdot 10^6$ gluinos will be produced, while in the SPS9 scenarios (heavier gluino of mass 1,275.2 GeV), $1.8 \cdot 10^4$ gluinos will be produced, according to our Fig. 10. Fore more realistic estimates, the NLO corrections would increase the cross sections for the various processes by a factor smaller than two. The above estimates, therefore, define a lower limit for the cross section and for the number of produced gluinos.

5 Conclusion

We started this article with a very brief review of the early phenomenology of photinos and gluinos to present our motivation for calculating the cross section for the production of both particles. We then highlighted certain difficulties in dealing with Majorana fermions like we treat Dirac fermions. One difficulty comes from the ambiguity in the definition of the internal propagators of the fermions; the other comes from the relative sign between the amplitudes. After that, we reviewed one method yielding the Feynman amplitudes when dealing with Majorana fermions, which makes the calculations as simple as the procedure for Dirac fermions. This method is based on a well-defined fermion flow and yields vertices equations without explicit charge–conjugation matrices. As illustrations, we

have presented examples showing how to calculate the photino and gluino production in pp collisions. We expect this review to help researchers who are new to the field of supersymmetric extensions of the standard model.

Acknowledgements This work was supported by CNPq; DBE supported by Master quota of CNPq from IF-UFRGS. We are grateful to Pierre Fayet, for several interesting information about photino and gluino phenomenology. One of us (MCR) is grateful to Howard E. Haber for bringing Ref. [28] to our attention, and to J. W. F. Valle for several interesting comments on leptogenesis.

References

1. Y.A. Gol'fand, E.P. Likhtman, ZhETF Pis. Red. **13**, 452 (1971)
2. Y.A. Gol'fand, E.P. Likhtman, JETP Lett. **13**, 323 (1971)
3. D.V. Volkov, V.P. Akulov, Phys. Lett. B **46**, 109 (1973)
4. J. Wess, B. Zumino, Nucl. Phys. B **70**, 39, (1974)
5. J. Wess, B. Zumino, Phys. Lett. B **49**, 52 (1974)
6. J. Wess, B. Zumino, Nucl. Phys. B **78**, 1 (1974)
7. P.A.M. Dirac, Proc. R. Soc. A **117**, 610, (1928)
8. P.A.M. Dirac, Proc. R. Soc. A **118**, 351, (1928)
9. E. Majorana, Nuovo Cim. **14**, 171 (1937)
10. J. Wess, J. Bagger, *Supersymmetry and Supergravity*, 2nd edn. (Princeton University Press, Princeton NJ, 1992)
11. M. Drees, R.M. Godbole, P. Royr, *Theory and Phenomenology of Sparticles*, 1st edn. (World Scientific Publishing Co. Pte. Ltd., Singapore, 2004)
12. H.J.W. Müller-Kirsten, A. Wiedemann, *Supersymmetry: An Introduction with Conceptual and Calculational Details*, 2nd edn. (World Scientific Publishing Co. Pte. Ltd., Singapore, 2010)
13. D. Bailin, A. Love, *Supersymmetric Gauge Field Theory and String Theory*, 1st edn. (Institute of Physics Publishing, Bristol UK, 1994)
14. H. Baer, X. Tata, *Weak Scale Supersymmetry*, 1st edn. (Cambridge University Press, UK, 2006)
15. I. Aitchison, *Supersymmetry in Particle Physics: An Elementary Introduction*, 1st edn. (Cambridge University Press, UK, 2007)
16. M. Srednicki, *Quantum field theory*, 4th edn. (Cambridge University Press, UK, 2010), arXiv:hep-th/0409035 and arXiv:hep-th/0409036
17. P. Fayet, Nucl. Phys. B **90**, 104 (1975)
18. P. Fayet, Phys. Lett. B **64**, 159 (1976)
19. P. Fayet, Phys. Lett. B **69**, 489 (1977)
20. P. Fayet, Phys. Lett. B **70**, 461 (1977)
21. P. Fayet, Nucl. Phys., B Proc. Suppl. **101**, 81 (2001) (Also in *Minneapolis 2000, 30 years of supersymmetry* 81–98)
22. M.C. Rodriguez, Int. J. Mod. Phys. A **25**, 1091 (2010)
23. H. Goldberg, Phys. Rev. Lett. **50**, 1419 (1983)
24. P. Fayet, Phys. Lett. B **86**, 272 (1979)
25. B.L. van der Waerden, Nachrichten Akad. Wiss. Göttingen, Math. Physik. Kl. **100** (1929)
26. H.E.Haber, arXiv:hep-ph/9405376
27. S.P. Martin, arXiv:1205.4076
28. H.K. Dreiner, H.E. Haber, S.P. Martin, Phys. Rep. **494**, 1 (2010)
29. H.J. Bhabha, Proc. R. Soc. A **154**, 195 (1935)
30. G.R. Farrar, P. Fayet, Phys. Lett. B **76**, 575 (1978)
31. G.R. Farrar, P. Fayet, Phys. Lett. B **79**, 442 (1978)
32. E. Cremmer, P. Fayet, L. Girardello, Phys. Lett. B **122**, 41 (1983)
33. P. Fayet, Phys. Lett. B **117**, 460 (1982)
34. H.E. Haber, G.L. Kane, Phys. Rep. **117**, 75 (1985)
35. S. Dawson, E. Eichten, C. Quigg, Phys. Rev. D **31**, 1581 (1985)
36. T. Kobayashi, M. Kuroda, Phys. Lett. B **139**, 208 (1984)
37. K. Grassie, P.N. Pandita, Phys. Rev. D **30**, 22 (1984)
38. J.D. Ware, M.E. Machacek, Phys. Lett. B **142**, 300 (1984)
39. L. Bento, J.C. Romao, A. Barroso, Phys. Rev. D **33**, 1488 (1986)
40. R. Basu, P.N. Pandita, C. Sharma, Phys. Rev. D **77**, 115009 (2008)
41. V.S. Berezinsky, E.V. Bugaev, E.S. Zaslavskaya, Nucl. Phys. B **272**, 193 (1986)
42. H. Baer, V.D. Barger, D. Karatas, X. Tata, Phys. Rev. D **36**, 96 (1987)
43. H. Baer, X. Tata, J. Woodside, Phys. Rev. D **42**, 1568 (1990)
44. H.E. Haber, G.L. Kane, Nucl. Phys. B **232**, 333 (1984)
45. E. Ma, G.G. Wong, Mod. Phys. Lett. A **3**, 1561 (1988)
46. R. Barbieri, G. Gamberini, G.F. Giudice, G. Ridolfi, Nucl. Phys. B **301**, 15 (1988)
47. G. Aad et al. [ATLAS Collaboration], Phys. Lett. B **701**, 186 (2011)
48. G. Aad et al. [ATLAS Collaboration], Phys. Lett. B **710**, 67 (2012)
49. G. Aad et al. [ATLAS Collaboration], arXiv:1208.3144 [hep-ex]
50. B.C. Allanach et al., Eur. Phys. J. C **25**, 113 (2002)
51. N. Ghodbane, H.-U. Martyn, arXiv:hep-ph/0201233
52. http://spa.desy.de/spa/
53. S.J.L. Rosner, Am. J. Phys. **71**, 302 (2003)
54. A.S. Kronfeld, C. Quigg, Am. J. Phys. **78**, 1081 (2010)
55. A. Denner, H. Eck, O. Hahn, J. Küblbeck, Nucl. Phys. B **387**, 467 (1992)
56. A. Denner, H. Eck, O. Hahn, J. Küblbeck, Phys. Lett. B **387**, 278 (1992)
57. E.I. Gates, K.L. Kowalski, Phys. Rev. D **45**, 1693 (1992)
58. T. Hahn, Comput. Phys. Commun. **140**, 418 (2001)
59. A. Bartl, H. Fraas, W. Majerotto, N. Oshimo, Phys. Rev. D **40**, 1594 (1989)
60. M.S. Carena, C.E.M. Wagner, Phys. Lett. B **195**, 599 (1987)
61. K.A. Olive, S. Rudaz, Phys. Lett. B **340**, 74 (1994)
62. http://www.linearcollider.org/
63. J.E. Brau et al. (ed.), *International Linear Collider Physics and detectors: 2011 Status Report*, CERN-LCD-NOTE-2011-038
64. W. Beenakker, R. Höpker, M. Spira, P.M. Zerwas, Nucl. Phys. B **492**, 51 (1997)
65. C.B. Mariotto, M.C. Rodriguez, Braz. J. Phys. **38**, 503, (2008), arXiv:0805.2094 [hep-ph]
66. D.B. Espindola, *Produção de Fotinos e Gluínos nas Extensões Supersimétricas da Eletrodinâmica Quântica e da Cromodinâmica Quântica*, (Master thesys defended at 03/18/2010)
67. W. Beenakker, M. Krämer, T. Plehn, M. Spira, P.M. Zerwas, Nucl. Phys. B **515**, 3 (1998)
68. T. Hahn, C. Schappacher, Comput. Phys. Commun. **143**, 54 (2002)
69. C.B. Mariotto, D.B. Espindola, M.C. Rodriguez, Phys. Rev. C **83**, 064902 (2011)
70. http://lhc.web.cern.ch/lhc/
71. J. Pumplin, D.R. Stump, J. Huston, H.L. Lai, P. Nadolsky, W.K. Tung, J. High Energy Phys. **207**, 12 (2002)